

## Quasinested Fe orbitals versus Mott-insulating V orbitals in superconducting $\text{Sr}_2\text{VFeAsO}_3$ as seen from angle-resolved photoemission

T. Qian,<sup>1</sup> N. Xu,<sup>1</sup> Y.-B. Shi,<sup>1</sup> K. Nakayama,<sup>2</sup> P. Richard,<sup>1,3</sup> T. Kawahara,<sup>2</sup> T. Sato,<sup>2,4</sup> T. Takahashi,<sup>2,3</sup> M. Neupane,<sup>5</sup> Y.-M. Xu,<sup>5</sup> X.-P. Wang,<sup>1</sup> G. Xu,<sup>1</sup> X. Dai,<sup>1</sup> Z. Fang,<sup>1</sup> P. Cheng,<sup>1</sup> H.-H. Wen,<sup>1</sup> and H. Ding<sup>1</sup>

<sup>1</sup>Beijing National Laboratory for Condensed Matter Physics, Institute of Physics, Chinese Academy of Sciences, Beijing 100190, China

<sup>2</sup>Department of Physics, Tohoku University, Sendai 980-8578, Japan

<sup>3</sup>WPI Research Center, Advanced Institute for Materials Research, Tohoku University, Sendai 980-8577, Japan

<sup>4</sup>TRiP, Japan Science and Technology Agency (JST), Kawaguchi 332-0012, Japan

<sup>5</sup>Department of Physics, Boston College, Chestnut Hill, Massachusetts 02467, USA

(Received 14 February 2011; revised manuscript received 11 April 2011; published 29 April 2011)

We have performed an angle-resolved photoemission spectroscopy study of the iron-based superconductor (SC)  $\text{Sr}_2\text{VFeAsO}_3$ . While V  $3d$  orbitals are found to be in a Mott-insulating state and show an incoherent peak at  $\sim 1$  eV below the Fermi level, the dispersive Fe  $3d$  bands form several hole- and electronlike Fermi surfaces (FSs), some of which are quasinested by the  $(\pi, 0)$  wave vector. This differs from the local-density approximation (LDA) calculations, which predict non-nested FSs for this material. However, LDA +  $U$  with a large effective Hubbard energy  $U$  on V  $3d$  electrons can reproduce the experimental observation reasonably well. The observed fermiology in SC  $\text{Sr}_2\text{VFeAsO}_3$  strongly supports that  $(\pi, 0)$  interband scattering between quasinested FSs may play an important role for SC in pnictides.

DOI: 10.1103/PhysRevB.83.140513

PACS number(s): 74.70.Xa, 74.25.Jb, 71.18.+y, 79.60.-i

The most important question for superconducting (SC) pnictides is how the low-energy electrons are paired. Since it occurs in the vicinity of the Fermi level  $E_F$ , the low-energy band structure and the fermiology are critical to the SC pairing. Angle-resolved photoemission spectroscopy (ARPES) showed that SC pnictides share similar fermiology, where holelike Fermi surfaces (FSs) near the Brillouin zone (BZ) center ( $\Gamma$ ) are quasinested to electronlike FSs at the  $M$  point by the  $(\pi, 0)$  wave vector [ $(\pi, \pi)$  in the folded BZ].<sup>1-3</sup> Inelastic neutron scattering measurements have revealed the presence of spin fluctuations near  $(\pi, 0)$  in several families of pnictides.<sup>4-6</sup> These experimental results confirm the importance of the interband scattering by the  $(\pi, 0)$  spin fluctuations in the pairing, suggesting the universality of pairing interactions in the pnictides.

However, the universality has encountered a serious challenge with the recent discovery of  $\text{Sr}_2\text{VFeAsO}_3$  (called 21311)<sup>7-9</sup> and  $\text{KFe}_2\text{Se}_2$ .<sup>10</sup>  $\text{KFe}_2\text{Se}_2$  behaves quite differently from other Fe-based SCs. This class shows very strong magnetism and localized features, and the origin of its high- $T_c$  SC is still intensively debated.<sup>11,12</sup> As for  $\text{SrVFeAsO}_3$ , most local-density approximation (LDA) band calculations, which have been quite reliable in calculating the FS of other pnictides, predicted that it has no good quasinested FS segments.<sup>13-16</sup>  $\text{Sr}_2\text{VFeAsO}_3$  can be regarded as a superlattice consisting of alternating stacking of  $\text{SrFe}_2\text{As}_2$  (called 122) and perovskitelike  $\text{Sr}_3\text{V}_2\text{O}_6$  layers. Compared with other pnictides, the most distinctive characteristic of  $\text{Sr}_2\text{VFeAsO}_3$  predicted by LDA calculations is the presence of metallic V  $3d$  bands. Although the V  $3d$  bands weakly couple to the Fe  $3d$  bands, small hybridization near  $E_F$  between them changes the FS topology and destroys the quasinesting condition.<sup>13</sup> Nevertheless, it is argued by one of the LDA papers<sup>14</sup> that if only the Fe-derived FS system is taken into account, the bare susceptibility shows a peak at  $(\pi, 0)$  similar to other pnictides. Furthermore, it has been pointed out that the V  $3d$  electrons

in  $\text{Sr}_2\text{VFeAsO}_3$  may be subject to strong on-site electron correlations that would remove V  $3d$  states from  $E_F$ .<sup>14</sup> Neutron diffraction measurements revealed antiferromagnetic ordering of the V sublattice, implying that strongly correlated vanadium may not contribute significantly to the FSs.<sup>17</sup> Thus, it is of particular importance to investigate the electronic structure and FS by performing ARPES measurements on  $\text{Sr}_2\text{VFeAsO}_3$ .

In this Rapid Communication, we present ARPES results on  $\text{Sr}_2\text{VFeAsO}_3$ . We find that the V  $3d$  orbitals are in a Mott-insulating state and show an incoherent peak or the lower Hubbard band (LHB) at a binding energy ( $E_B$ ) of  $\sim 1$  eV. All the dispersive bands within 0.8 eV below  $E_F$  can mostly be attributed to Fe  $3d$  states. The observed FS topology is essentially similar to those of other pnictide SCs and suggests the importance of the  $(\pi, 0)$  interband scattering for the pairing in  $\text{Sr}_2\text{VFeAsO}_3$ .

High-quality single crystals of  $\text{Sr}_2\text{VFeAsO}_3$  ( $T_c \sim 37$  K) were grown by the flux method. ARPES measurements were performed at beamline 28A of the Photon Factory (KEK, Tsukuba), beamline U-71A of the Synchrotron Radiation Center (Stoughton, WI), and Tohoku University using the He  $I\alpha$  resonance line ( $h\nu = 21.2$  eV). The energy and angular resolutions were set to 30 meV and  $0.2^\circ$ , respectively. Samples with the tiny size of  $< 0.2 \times 0.2$  mm<sup>2</sup> were carefully mounted using a robotic mounting device, cleaved *in situ*, and measured at 40 K in a working vacuum better than  $1 \times 10^{-10}$  Torr. As the cleavage may take place between the two equivalent SrO layers with the longest bond, the cleaved surface is nonpolarized, preventing the appearance of a surface state as in other vanadates.<sup>18-20</sup> The  $E_F$  of the samples was referenced to that of a gold film evaporated onto the sample holders.

As pointed out by LDA calculations, the valence of V ions is important to the fermiology of  $\text{Sr}_2\text{VFeAsO}_3$ . To determine the valence of V in  $\text{Sr}_2\text{VFeAsO}_3$ , we have measured a core-level spectrum at  $h\nu = 220$  eV, as shown in Fig. 1(a). We identify a broad V  $3s$  peak at  $E_B \sim 70$  eV and a V  $3p$  peak whose

leading edge at the lower- $E_B$  side is at 37.2 eV. The broad line shape of the 3s peak in  $\text{Sr}_2\text{VFeAsO}_3$  is more similar to those in  $\text{V}_2\text{O}_3$  and  $\text{VO}_2$  than the one in  $\text{V}_2\text{O}_5$ , which is much narrower due to the disappearance of the multiple splitting in the  $d^0$  configuration.<sup>21</sup> The leading edge of the V 3p peak (37.2 eV) in  $\text{Sr}_2\text{VFeAsO}_3$  is also closer to those in  $\text{V}_2\text{O}_3$  (37.8 eV) and  $\text{VO}_2$  (39.5 eV) than the one in  $\text{V}_2\text{O}_5$  (40.5 eV).<sup>21</sup> These results suggest that the valence of V is near 3+ or 4+, which means that the V 3d orbitals are partially filled and will contribute to the VB. To clarify the nature of the V 3d states, we performed photon energy dependence measurements of the VB at the normal-emission direction. As seen in Fig. 1(b), there is a broad peak centered at 1 eV that is not observed in other pnictides. As noticed before, photoemission spectra of many vanadium oxides exhibit a broad peak around 1 eV, which has been attributed to the LHB due to strong correlations between V 3d electrons.<sup>21–24</sup> The 1-eV peak height shows a different photon energy dependence compared with another prominent peak at 0.32 eV, suggesting that they have different origins. To quantitatively compare their photon energy dependence, we extracted the spectral intensity of the two peaks by using the expression  $I = I_A + I_B + I_{bg}$ . Here,  $I_A$  and  $I_B$  represent the intensity of the two asymmetric peaks at 1 and 0.32 eV, respectively, using the Doniach-Sunjić line shape, and  $I_{bg}$  is a Shirley-type background. All the spectra are well fitted within the [0.3, 2 eV] range, except for those near  $h\nu = 53$  eV, where the 0.32-eV peak is strongly suppressed. The intensities of the two peaks obtained from the fitting curves are plotted as a function of photon energy in Fig. 1(c). In Fig. 1(c), we also plot the photon energy dependence of the spectral intensity at  $E_F$ . Both the 0.32-eV peak and the  $E_F$  intensity show a remarkable Fe 3p-3d antiresonance dip around 53 eV, as

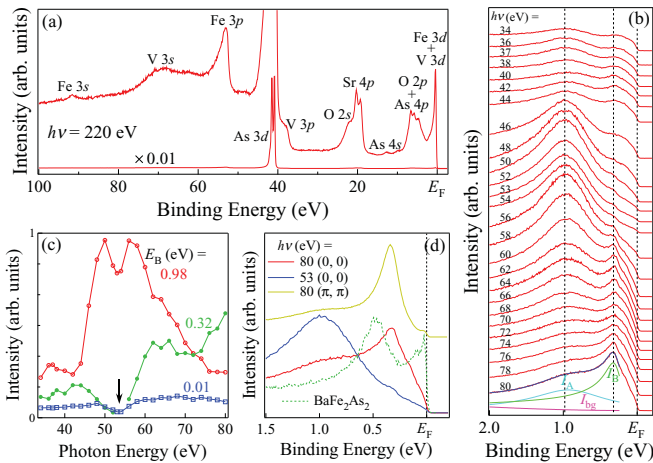


FIG. 1. (Color online) (a) Core-level photoemission spectrum at  $h\nu = 220$  eV. Associated atomic orbitals are indicated. To completely show the strong peaks from the As 3d orbital, the spectrum divided by 100 is also plotted. (b) Valence band (VB) at the BZ center measured at different photon energies (34–80 eV). All the spectra are normalized by the photon flux. The fitting curves for the spectrum at  $h\nu = 80$  eV are also shown. (c) Photon energy dependence of the intensities of the two peaks obtained from the fitting curves and the spectral intensity at  $E_B = 0.01$  eV. (d) Direct comparison of the VB measured at  $h\nu = 53$  and 80 eV, along with the VB of  $\text{BaFe}_2\text{As}_2$  ( $h\nu = 80$  eV).

observed in  $\text{Ba}_{0.6}\text{K}_{0.4}\text{Fe}_2\text{As}_2$ ,<sup>25</sup> suggesting that the structures at 0.32 eV and near  $E_F$  are mostly from Fe 3d orbitals. As the photon energy reaches the V 3p-3d absorption threshold of 38 eV, the 1-eV peak shows an enhancement with a Fano-like resonance profile, suggesting that it corresponds mostly to the incoherent part of V 3d states.<sup>23</sup> We further compare the spectra measured at 80 and 53 eV in Fig. 1(d). At  $h\nu = 53$  eV where the Fe-3d intensity is strongly suppressed, no dispersive feature that could be attributed to the coherent V 3d band is observed in the vicinity of  $E_F$ . Instead, there is only a broad 1-eV peak that is likely the incoherent V 3d peak, indicating that V 3d orbitals are in a Mott-insulating state.

After clarifying the insulating nature of the V 3d states, we turn to resolve the low-energy band dispersion. Figures 2(a)–2(c) show ARPES spectra along  $\Gamma M$ ,  $\Gamma X$ , and  $MX$  in the second BZ, respectively, where the spectral intensity is found to be much more enhanced as compared to the one in the first BZ. While the 1-eV peak of the incoherent V 3d orbitals shows little dispersion, the lower-energy features are strongly dispersive. To better track the band dispersion, we plot the intensity of second derivatives of the energy distribution curves (EDCs) along the high symmetry lines  $\Gamma$ -X-M- $\Gamma$  in Fig. 2(e). To overcome the failure of simple LDA calculations in predicting the Mott-insulating V bands, we adopt a simple LDA + U approach to study this material, in which we only consider the correlation effects of V 3d electrons as an effective Hubbard energy  $U$ . We found that the V 3d bands are obviously pushed away from  $E_F$  as  $U$  is increased and develop an insulating gap for  $U \geq 4$  eV. When  $U$  reaches 6 eV, the LHB is around 1 eV similar to what is observed experimentally. We plot the LDA + U results using experimental lattice parameters with the optimized internal coordinates of As in Fig. 2(e) and further renormalize the

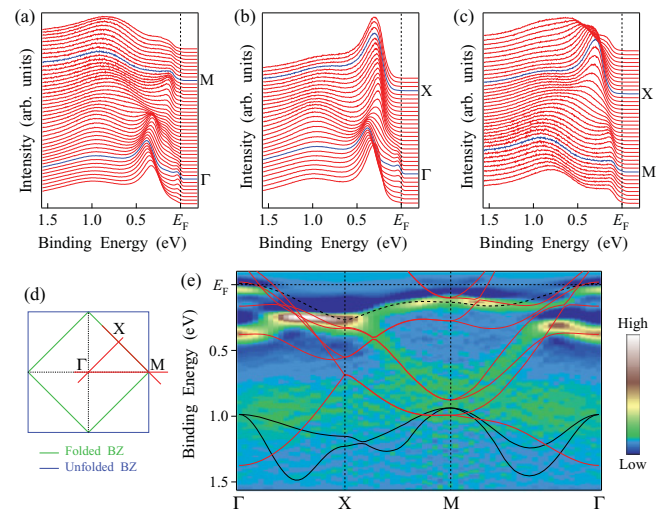


FIG. 2. (Color online) Dispersive EDCs along (a)  $\Gamma M$ , (b)  $\Gamma X$ , and (c)  $MX$  measured at  $h\nu = 80$  eV. (d) Schematic BZ indicating measurement locations for panels (a)–(c). (e) Second derivative plot along  $\Gamma X M \Gamma$ . LDA + U bands are also plotted for comparison. The Fe 3d bands (red/gray lines) are renormalized by a factor of 1.6, whereas the V 3d bands (black lines) are not. The Fe 3d<sub>xy</sub> band (black dashed line) is renormalized by a factor of 3.3 to reproduce the experimental band near  $E_F$ .

Fe  $3d$  bands by a factor of 1.6 to match the overall band dispersion below 1 eV. In particular, the highly dispersive band with its bottom at  $M$  is well reproduced by the renormalized calculations. While the renormalized band calculations fit the measured bands well at high  $E_B$ , we find discrepancies at lower energy. The near- $E_F$  band can be well reproduced by renormalizing the Fe  $3d_{xy}$  band ( $x$  and  $y$  axes along  $\Gamma M$ ) by a factor of 3.3, indicating energy- or orbital-dependent band renormalization effects similar to what is observed in  $\text{Ba}_{0.6}\text{K}_{0.4}\text{Fe}_2\text{As}_2$ ,<sup>25</sup> possibly due to the correlation effect of Fe  $3d$  electrons.

In order to resolve the detailed structure of the bands in the vicinity of  $E_F$ , we have performed fine-step ARPES measurements within 0.5 eV below  $E_F$ . Figure 3 shows the EDC plots [(a) and (d)], the intensity plots [(b) and (e)], and the second derivative plots [(c) and (f)] of ARPES spectra in the vicinity of  $\Gamma$  and  $M$ , respectively. As seen in Figs. 3(a)–3(c), two holelike bands at  $\Gamma$  are observed. While the inner  $\Gamma$ -centered band barely crosses  $E_F$ , the outer one forms a small holelike FS. Figures 3(d)–3(f) clearly display one electronlike band around  $M$ . From the dispersive band, a Fermi velocity of  $0.57 \pm 0.05$  eV  $\text{\AA}$  is obtained, which is 2.7 times smaller than the value extracted from the nonrenormalized LDA + U calculations.

Figure 4(a) shows the ARPES intensity plot at  $E_F$  at  $h\nu = 80$  eV obtained by assuming a fourfold symmetry for the full BZ. We clearly observe one small hole pocket at  $\Gamma$  and two electron pockets at  $M$ . In addition, another large hole pocket centered at  $\Gamma$  is observed by using the He I $\alpha$  line, as shown in Fig. 4(b), in agreement with our LDA + U calculations. The absence of that band at  $h\nu = 80$  eV [Figs. 3(a)–3(c)] is most likely due to matrix element effects. In Fig. 4(c), we summarize the four observed FS pockets by using the  $k_F$  points extracted from the MDCs and obtained from the fourfold symmetry operations. While the holelike

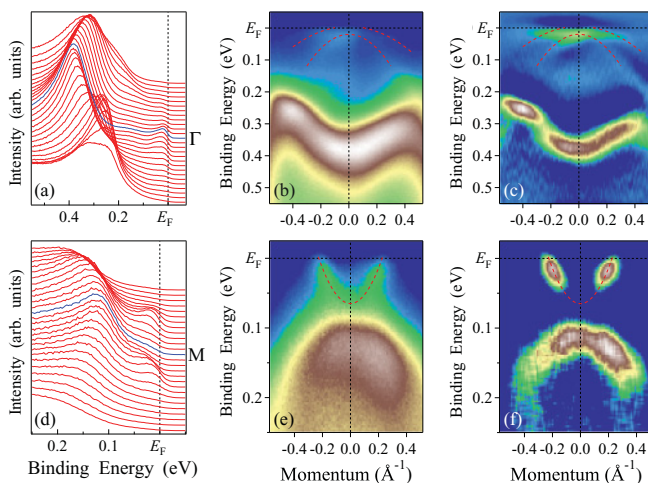


FIG. 3. (Color online) (a) EDCs, (b) intensity plot, and (c) second derivative plot in the vicinity of  $E_F$  at  $\Gamma$  measured at  $h\nu = 80$  eV. (d)–(f) same as in panels (a)–(c) but taken at  $M$ . The second derivatives of EDCs are used in panel (c). We summed the second derivatives of EDCs and momentum distribution curves (MDCs) in panel (f) to better track the fast dispersive band near  $E_F$  at  $M$ . Red dashed lines are guides for eyes.

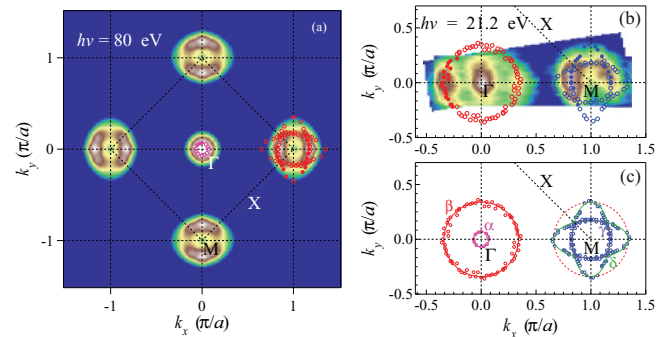


FIG. 4. (Color online) ARPES intensity plot at  $E_F$  as a function of the two-dimensional wave vector measured at (a)  $h\nu = 80$  and (b) 21.2 eV (He I $\alpha$  line). The intensity at  $E_F$  is obtained by integrating the spectra within  $\pm 20$  meV with respect to  $E_F$ . Filled circles show experimentally determined  $k_F$  points, and open circles represent  $k_F$  points symmetrized by assuming a fourfold symmetry with respect to  $\Gamma$  and  $M$ . (c) Extracted FSs (solid lines) from the extracted  $k_F$  points. The dashed FS is the  $\beta$  FS shifted by the  $(\pi, 0)$  wave vector.

$\alpha$  and  $\beta$  FSs centered at  $\Gamma$  have areas of 0.7% and 18% of the BZ, the electronlike  $\gamma$  and  $\delta$  FSs at  $M$  have areas of 5% and 13%, respectively. According to the Luttinger theorem on two-dimensional FS sheets, which are well expected given the superlattice-like structure in this material, the four FS sheets correspond to a valence of Fe ions close to 2+, like other parent iron pnictides. From this valence of Fe ions, it is inferred that V has a 3+ -valence state, consistent with the core-level measurement. As shown in Fig. 4(c), the  $\beta$  FS, when shifted by the  $(\pi, 0)$  wave vector, overlaps well with the  $\delta$  FS. Such a FS topology is very similar to those observed in other optimally doped SC pnictides. Since SC in many pnictides is thought to be related to  $(\pi, 0)$  interband scattering between hole and electron pockets, the similar fermiology observed here implies that  $(\pi, 0)$  interband scattering between quasinested FSs may play an important role to SC in  $\text{Sr}_2\text{VFeAsO}_3$ .

Although the fermiology in  $\text{Sr}_2\text{VFeAsO}_3$  is qualitatively similar to those of other pnictides, we observe some marked differences.  $\text{Sr}_2\text{VFeAsO}_3$  shows very large FSs, and the nesting occurs only between the outer hole and the electron pockets. Many band calculations have pointed out that the relative positions of the low-energy bands as well as the fermiology is very sensitive to the As height from the Fe plane ( $h_{\text{As}}$ ). The  $h_{\text{As}}$  in  $\text{Sr}_2\text{VFeAsO}_3$  is increased by 5% compared with that in  $\text{SrFe}_2\text{As}_2$ .<sup>7,26</sup> According to the band calculations,<sup>27,28</sup> such an increase will reduce the hopping integral for the  $3d_{xy}$  orbital via the Fe-As bond, which pushes up the  $3d_{xy}$  band at  $\Gamma$ . Therefore, the large hole pocket in  $\text{Sr}_2\text{VFeAsO}_3$  may originate from the Fe  $3d_{xy}$  orbital due to the increase of  $h_{\text{As}}$ .<sup>29</sup> Assuming that the outer electronlike FS originates from the Fe  $3d_{xy}$  orbital,<sup>27,28</sup> the nesting closely related to the SC may be the intra- $d_{xy}$  orbital in  $\text{Sr}_2\text{VFeAsO}_3$ .

Unlike the increase of  $h_{\text{As}}$  in  $\text{Sr}_2\text{VFeAsO}_3$ , in another 21311 compound,  $\text{Sr}_2\text{ScFeAsO}_3$ , the  $h_{\text{As}}$  is even slightly smaller than that in  $\text{SrFe}_2\text{As}_2$ .<sup>26,30</sup> The variation in  $h_{\text{As}}$  is naturally attributed to the strain from the perovskitelike intercalated block, which is controlled by the radius of the transition-metal ions. In contrast to SC  $\text{Sr}_2\text{VFeAsO}_3$ ,  $\text{Sr}_2\text{ScFeAsO}_3$ , in which the  $\text{Sr}_3\text{Sc}_2\text{O}_6$  intercalated block is considered as a band insulator,

shows a semiconducting behavior.<sup>30,31</sup> Such differences may arise from significant differences in the fermiology sensitive to  $h_{As}$ . It is noticed that applied pressure leads to the appearance of SC in BaFe<sub>2</sub>As<sub>2</sub>, which may be understood based on the change of orbital characters of the quasineesting FSs due to structural changes.<sup>32</sup> Since the  $h_{As}$  in 21311 can be tuned easily by changing the transition-metal elements, the 21311 system provides a good opportunity to study, by ARPES, the relationship among SC, electronic structure, and crystal structure.

Remarkably, the spectral line shape of Sr<sub>2</sub>VFeAsO<sub>3</sub> is quite different from that of many other pnictides. As seen in Fig. 1(d), the intensity near  $E_F$  is strongly suppressed compared with the VB, whereas, the  $E_F$  intensity is comparable with the VB in BaFe<sub>2</sub>As<sub>2</sub>. Interestingly, the suppression of spectral intensity only occurs within  $\sim 0.1$  eV below  $E_F$ , while the band renormalization near  $E_F$  and the Fermi velocities are not significantly different from those of Ba<sub>0.6</sub>K<sub>0.4</sub>Fe<sub>2</sub>As<sub>2</sub>.<sup>25</sup> This can be attributed to a strong momentum dependence of the

self-energy as long-range interactions become important in the vicinity of a Mott transition.<sup>24</sup> Similar physics is found in the ruthenates in which an orbital-selective Mott transition takes place.<sup>33–35</sup> Our ARPES results suggest that the itinerant Fe 3d states in Sr<sub>2</sub>VFeAsO<sub>3</sub> may be pushed toward a Mott transition with the insertion of the Mott-insulating Sr<sub>3</sub>V<sub>2</sub>O<sub>6</sub> layers, while the microscopic origin of the possible long-range interactions remains unclear. With only very little hybridization between Fe 3d and V 3d states, Sr<sub>2</sub>VFeAsO<sub>3</sub> can be regarded as a model compound for such an exotic phenomenon.

This work was supported by grants from CAS (Grant No. 2010Y1JB6), NSFC (Grants No. 11004232 and No. 11050110422), MOST of China (Grant No. 2010CB923000), JSPS, TRIP-JST, CREST-JST, MEXT of Japan, and NSF, DOE of the United States. This work is based upon research conducted at the SRC supported by NSF Grant No. DMR-0537588 and the PF supported by Grant No. PF-PAC 2009S2-005.

- 
- <sup>1</sup>H. Ding *et al.*, *Europhys. Lett.* **83**, 47001 (2008).  
<sup>2</sup>K. Terashima *et al.*, *Proc. Natl. Acad. Sci. USA* **106**, 7330 (2009).  
<sup>3</sup>K. Nakayama *et al.*, *Phys. Rev. Lett.* **105**, 197001 (2010).  
<sup>4</sup>A. D. Christianson *et al.*, *Nature (London)* **456**, 930 (2008).  
<sup>5</sup>H. A. Mook *et al.*, e-print arXiv:0904.2178.  
<sup>6</sup>D. S. Inosov *et al.*, *Nat. Phys.* **6**, 178 (2010).  
<sup>7</sup>X. Y. Zhu, F. Han, G. Mu, P. Cheng, B. Shen, B. Zeng, and H.-H. Wen, *Phys. Rev. B* **79**, 220512 (2009).  
<sup>8</sup>F. Han *et al.*, *Sci. China, Ser. G* **53**, 1202 (2010).  
<sup>9</sup>H. Kotegawa *et al.*, *J. Phys. Soc. Jpn.* **78**, 123707 (2009).  
<sup>10</sup>J. G. Guo, S. Jin, G. Wang, S. Wang, K. Zhu, T. Zhou, M. He, and X. Chen, *Phys. Rev. B* **82**, 180520(R) (2010).  
<sup>11</sup>T. Qian *et al.*, e-print arXiv:1012.6017.  
<sup>12</sup>X.-P. Wang *et al.*, *Europhys. Lett.* **93**, 57001 (2011).  
<sup>13</sup>K. W. Lee and W. E. Pickett, *Europhys. Lett.* **89**, 57008 (2010).  
<sup>14</sup>I. I. Mazin, *Phys. Rev. B* **81**, 020507 (2010).  
<sup>15</sup>I. R. Shein and A. L. Ivanovskii, *J. Supercond. Novel Magn.* **22**, 613 (2009).  
<sup>16</sup>G. T. Wang, M. Zhang, L. Zheng, and Z. Yang, *Phys. Rev. B* **80**, 184501 (2009).  
<sup>17</sup>M. Tegel, T. Schmid, T. Stürzer, M. Egawa, Y. Su, A. Senyshyn, and D. Johrendt, *Phys. Rev. B* **82**, 140507 (2010).  
<sup>18</sup>A. Sekiyama *et al.*, *Phys. Rev. Lett.* **93**, 156402 (2004).  
<sup>19</sup>A. Liebsch, *Phys. Rev. Lett.* **90**, 096401 (2003).  
<sup>20</sup>I. A. Nekrasov, G. Keller, D. E. Kondakov, A. V. Kozhevnikov, T. Pruschke, K. Held, D. Vollhardt, and V. I. Anisimov, *Phys. Rev. B* **72**, 155106 (2005).  
<sup>21</sup>R. Zimmermann *et al.*, *J. Phys. Condens. Matter* **10**, 5697 (1998).  
<sup>22</sup>K. Maiti and D. D. Sarma, *Phys. Rev. B* **61**, 2525 (2000).  
<sup>23</sup>S. Shin, S. Suga, M. Taniguchi, M. Fujisawa, H. Kanzaki, A. Fujimori, H. Daimon, Y. Ueda, K. Kosuge, and S. Kachi, *Phys. Rev. B* **41**, 4993 (1990).  
<sup>24</sup>I. H. Inoue, I. Hase, Y. Aiura, A. Fujimori, Y. Haruyama, T. Maruyama, and Y. Nishihara, *Phys. Rev. Lett.* **74**, 2539 (1995).  
<sup>25</sup>H. Ding *et al.*, *J. Phys.: Condens. Matter* **23**, 135701 (2011).  
<sup>26</sup>M. Tegel *et al.*, *J. Phys. Condens. Matter* **20**, 452201 (2008).  
<sup>27</sup>V. Vildosola, L. Pourovskii, R. Arita, S. Biermann, and A. Georges, *Phys. Rev. B* **78**, 064518 (2008).  
<sup>28</sup>K. Kuroki, H. Usui, S. Onari, R. Arita, and H. Aoki, *Phys. Rev. B* **79**, 224511 (2009).  
<sup>29</sup>The small FS area of the Fe 3d<sub>xy</sub> orbital in our calculations in Fig. 2(e) is due to the smaller  $z_{As}$ , 10% lower than the experimental value.  
<sup>30</sup>H. Ogino *et al.*, *Supercond. Sci. Technol.* **22**, 085001 (2009).  
<sup>31</sup>G. F. Chen *et al.*, *Supercond. Sci. Technol.* **22**, 072001 (2009).  
<sup>32</sup>S. A. J. Kimber *et al.*, *Nature Mater.* **8**, 471 (2009).  
<sup>33</sup>M. Neupane, P. Richard, Z.-H. Pan, Y.-M. Xu, R. Jin, D. Mandrus, X. Dai, Z. Fang, Z. Wang, and H. Ding, *Phys. Rev. Lett.* **103**, 097001 (2009).  
<sup>34</sup>V. I. Anisimov *et al.*, *Eur. Phys. J. B* **25**, 191 (2002).  
<sup>35</sup>A. Liebsch, *Phys. Rev. Lett.* **91**, 226401 (2003).